International Journal of Nanomedicine

Dovepress
Taylor & Francis Group

Open Access Full Text Article

ORIGINAL RESEARCH

Enhanced Long-Term Antibacterial and Osteogenic Properties of Silver-Loaded Titanium Dioxide Nanotube Arrays for Implant Applications

Yicun Yao[1,2], Peifen Lin[1], Dongping Ye[1], Haixiong Miao[1], Lin Cao[3], Peng Zhang[3], Jiake Xu[4,5], Libing Dai[1,2]

[1]Department of Orthopedics, Guangzhou Red Cross Hospital, Guangzhou Red Cross Hospital of Jinan University, Guangzhou, Guangdong, 510220, People's Republic of China; [2]Guangzhou Institute of Traumatic Surgery, Guangzhou Red Cross Hospital, Guangzhou Red Cross Hospital of Jinan University, Guangzhou, Guangdong, 510220, People's Republic of China; [3]Institute of Advanced Wear & Corrosion Resistant and Functional Materials, National Joint Engineering Research Center of High Performance Metal Wear Resistant Materials Technology, Jinan University, Guangzhou, 510632, People's Republic of China; [4]Faculty of Pharmaceutical Sciences, Shenzhen University of Advanced Technology, ShenZhen, Guangdong, 518107, People's Republic of China; [5]School of Biomedical Sciences, The University of Western Australia, Perth, 6009, Australia

Correspondence: Peng Zhang; Libing Dai, Email tzhangpeng@jnu.edu.cn; libingdai@ext.jnu.edu.cn

Objective: This study explored constructing silver-loaded titanium dioxide nanotube (TiO_2 NT) arrays on titanium surfaces using anodic oxidation combined with ion implantation. We assessed the cytocompatibility, antibacterial properties, and osteogenic potential of these silver-loaded TiO_2 NT arrays, along with the underlying mechanisms.

Methods: We utilized anodization to create TiO_2 NT arrays and employed ion implantation to load silver ions, categorizing samples into groups NT-Ag-II-L, NT-Ag-II-M, and NT-Ag-II-H based on different Ag ion dosages. Characterization was performed via scanning electron microscopy (SEM). We evaluated cell compatibility and assessed the antimicrobial performance and Ag ion release profiles. The osteogenic ability of the samples was measured, and the effects on ERK5 and osteogenesis-related factors were analyzed. To clarify the role of ERK5 in osteogenesis, we inhibited the ERK5 pathway using BIX02188 and subsequently re-evaluated osteogenic capacity in co-cultured cells.

Results: SEM analysis showed that in the NT-Ag-II-M group, Ag ions exhibited a flake-like distribution atop the TiO_2 NTs, while NT-Ag-II-L and NT-Ag-II-H groups presented clustered grid structures. Energy-filtered transmission electron microscopy (EFTEM) confirmed orderly Ag ion arrangements within the lumens of the nanotubes. Notably, the silver-loaded TiO_2 NT arrays did not inhibit MC3T3-E1 cell proliferation and enhanced early cellular adhesion. All samples displayed significant antimicrobial activity initially, which decreased after seven days; however, Ag ion release decreased gradually over the first 14 days before stabilizing. Additionally, the samples increased alkaline phosphatase activity, collagen secretion, and extracellular matrix mineralization, up-regulating ERK5 and other osteogenic factors. Inhibition of the ERK5 pathway suppressed the osteogenic capabilities of the samples.

Conclusion: Anodization and ion implantation successfully produced silver-loaded TiO_2 NT arrays on titanium surfaces, demonstrating no cytotoxicity, sustained antimicrobial properties, and enhanced osteogenic potential. The antimicrobial effect relates to silver ion release, whereas osteogenesis is promoted by ERK5 signaling triggered by silver ions.

Keywords: titanium, implant associated infection, silver ion, ion implantation, antibacterial properties, osseointegration, ERK5

Introduction

With the escalating elderly population, there is an increasing demand for the orthopedic surgery.[1] Titanium and titanium alloys are extensively utilized in orthopedic implants due to their exceptional mechanical properties and biocompatibility in physiological environments.[2] Nevertheless, the prevalence of implant-associated infections is on the rise as titanium implants becomes more widespread.[3] Furthermore, studies have demonstrated that titanium and its alloys exhibit restricted osteogenic activity, which could potentially result in implant loosening.[4] Implant failure is mostly caused by implant-associated infections and loosening of the implant, which can lead to a number of consequences such as patient

Received: 29 August 2024
Accepted: 22 February 2025
Published: 24 March 2025

Graphical Abstract

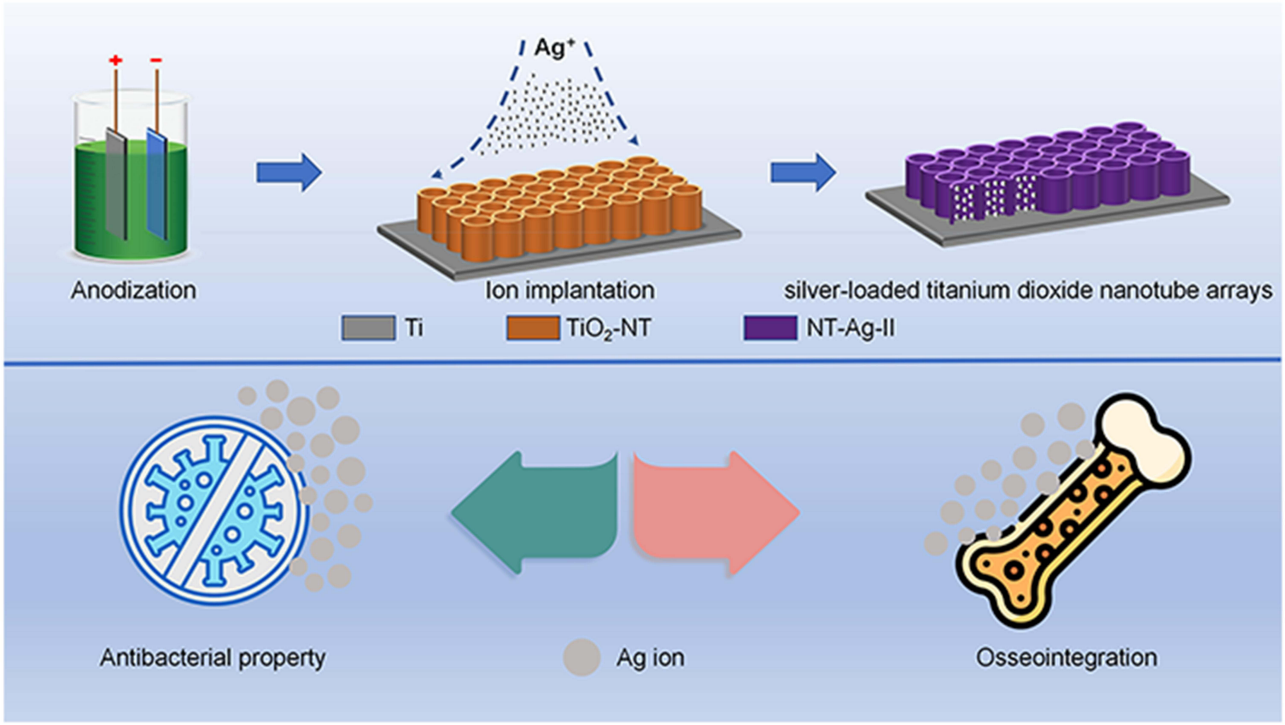

discomfort, implant failure, prolonged hospitalization, financial burden, and even death, posing a severe risk to individuals.[5] According to above, a titanium-based material possessing both osteogenic activity and antibacterial properties is desperately need in clinical practice.

To address these obstacles, a variety of strategies have been implemented, with a particular emphasis on the modification of implantable material surfaces.[2,6] Titanium dioxide nanotubes are a commonly used surface modification method for titanium metal.[7] Compared to other silver based coatings, it can not only increase the dosage of drug loading, but also achieve sustained release of drugs. The unique microstructure of titanium dioxide nanotubes has both inhibitory effects on bacterial growth and promoting effects on the adhesion, migration, and proliferation of osteoblasts.[8–10] Additionally, titanium dioxide nanotubes have a large specific surface area, making them an ideal drug carrier that can achieve sustained drug release.[11] Anodization is a recognized simple, economical, and highly operable process for constructing nanoscale morphology on titanium metal surfaces, and it allows for in-situ growth of TiO_2 nanotubes with good adhesion to the titanium foil.[12]

Ag ions are widely used in clinical settings as inorganic antimicrobial agents due to their strong antibacterial properties, broad spectrum, and non-resistance characteristics.[13] However, some previous studies have the drawback of sudden release of silver ions, which may pose a risk to biological safety and the problem of short maintenance time of antibacterial effects.[14] Due to the degradation of biological materials and ion burst release, other silver ion implantation methods have the problem of short antibacterial effect time. However, one month after surgery is a high-risk period for postoperative infection in internal plants. Therefore, how to control the long-term and effective release of silver ions remains a challenge. Ion implantation is a surface modification method that incorporates ions into solid surfaces. Through ion implantation, ions can be uniformly and stably incorporated into the target material's surface. Compared to other doping methods, ion implantation offers higher purity of doped ions and a tighter and more stable bond with the substrate. Due to the close binding between ions and the substrate, the release rate of ions in solution slows down after ion implantation.[15,16] This not only improves the biocompatibility of Ag ion implantation but also achieves the effect of sustained Ag ion release, leading to long-lasting antimicrobial properties.

Studies have indicated that the MAPK signaling pathway plays an indispensable role in osteoblast differentiation. More significantly, the MAPK pathway interacts with various signaling pathways such as BMP and Wnt, thereby emerging as a crucial signaling pathway in regulating osteogenesis. ERK5, as an atypical member of the MAPK family, also plays a pivotal role in osteogenic regulation. Nevertheless, it remains unclear whether the ERK5 signaling pathway mediates the osteogenic effect of silver ion-loaded titanium dioxide nanotube arrays.

Herein, we employed anodization to generate nanotubes on the titanium surface and implemented a metal vapor vacuum arc to securely embed Ag ions in situ. The aim was to investigate the potential clinical applications of TiO_2 nanotubes loaded with Ag ions in terms of their osteogenic activity and antibacterial efficacy.

Preventing implant-associated infections is crucial for the success of orthopedic surgery. In this study, the surface of a titanium foil was modified through anodic oxidation and the addition of Ag ions. Following ion implantation at levels of 1.0×10^{17} ions/cm^2, 5.0×10^{17} ions/cm^2, and 1.0×10^{18} ions/cm^2, titanium dioxide nanotube arrays were formed with variable concentrations of Ag ions. The antimicrobial properties and osteogenic activity of the titanium foil were evaluated both prior to and following its embedding.

Materials and Methods

Preparation of TiO_2 Nanotube by Anodic Oxidation

The pure Ti foil was cut into sizes of 1cm×3cm. It underwent ultrasonic cleaning for 5 minutes in acetone, ethanol, and deionized water, respectively, followed by air drying for subsequent procedures. Subsequently, the Ti foil was subjected to electrochemical anodization to generate TiO_2 nanotubes. The electrolyte used had the following composition: NH_4F (0.3 wt. %), deionized H_2O (2.0 vol. %), and glycol (98 vol. %). Pure titanium foil served as the anode, while a stainless steel sheet acted as the cathode under constant temperature conditions on a magnetic stirrer. The power parameter was set at 40V, and the reaction duration was 1 hour. After anodization, the samples were rinsed again with deionized water, followed by ultrasonic cleaning to remove any residual impurities from the surface.

Ag Ions Implantation

Ag ions were incorporated into the TiO_2 nanotube arrays using metal vapor vacuum arc implantation with an accelerating voltage of 60 kV and different doses of Ag ions implantation. The implantation doses of Ag ions were 1.0×10^{17} ions/cm^2, 5.0×10^{17} ions/cm^2, and 1.0×10^{18} ions/cm^2, respectively, which were abbreviated as NT-Ag-II-L, NT-Ag-II-M, and NT-Ag-II-H. Consequently, a titanium dioxide nanotube array loaded with Ag ions was obtained. As a comparison, TiO_2 nanotube arrays without ion implantation were utilized as the control group, denoted as TiO_2-NT.

Sample Characterization

The morphological observations of the the TiO_2 nanotube arrays and silver-loaded titanium dioxide nanotube arrays were conducted using a field-emission scanning electron microscope (FE-SEM, Zeiss, Oberkochen, Germany) at an accelerating voltage of 10 kV. Following a 30-minute ultrasonic cleaning in ethanol, the morphology and dispersion of the prepared sample were examined using high-resolution transmission electron microscopy (HRTEM, JEM-2100, JEOL, Japan).

Cell Culture of MC3T3-E1

The growth medium used in this study consisted of 10% fetal bovine serum (HyClone, South Logan, UT), α-minimum essential medium (α-MEM; Gibco Invitrogen, Inc., Carlsbad, CA), 0.3 mg/mL glutamine (HyClone), 100 μg/mL streptomycin, and 100 U/mL penicillin. MC3T3-E1 cells (Stem Cell Bank, Chinese Academy of Sciences, Shanghai, China) were cultured in this standard growth medium and maintained in a thermostat at 37 °C with constant humidity. For the subsequent assays, third-generation MC3T3-E1 cells were utilized. The samples were placed in 6-well or 24-well plates (Costar) accordingly, and cells were seeded at varying densities to meet the specific experimental requirements.

Cytocompatibility Evaluation

To assess the cytotoxicity of the Ag ions implantation and evaluate the cell compatibility of the samples, the proliferation of MC3T3-E1 cells was measured using the methyl thiazolyl tetrazolium (MTT) method. The samples were placed in a 24-well plate followed by seeding the MC3T3-E1 cell suspension at a concentration of 5×10^3 cells per 100 μL. The plate was then incubated in a CO_2 incubator at 37 °C for 1–7 days. After the incubation period, MTT reagent (20 μL) was added to each well and further incubated for 4 hours. The supernatant was subsequently removed, and 150 μL dimethyl sulfoxide (DMSO) was added to each well. The mixture was shaken for approximately 10–15 minutes. Finally, the absorbance (OD) value at 495 nm of each group was measured using an enzyme-labeled instrument (BioTek INstruments ELx800).

Cell Adhesion

To examine cell adhesion on the sample surfaces, the samples were placed in a 6-well plate and seeded with MC3T3-E1 cell suspension at a concentration of 5×10^3 cells per 100 μL. After 24 hours of incubation, the samples were carefully removed from the wells and washed with preheated phosphate-buffered saline (PBS) at 37 °C. The cytoskeleton of the MC3T3-E1 cells was stained using FITC-Phalloidin (Sigma USA). Subsequently, a confocal laser scanning microscope (CLSM) from Zeiss, Germany, was utilized to observe the cytoskeleton of the MC3T3-E1 cells.

Plate-Counting Method

The plate-counting method was employed to evaluate the in vitro antibacterial activity of the samples against Gram-positive Staphylococcus aureus (S. aureus, ATCC6538) and Gram-negative Escherichia coli (E. coli, ATCC10536). The bacteria were inoculated in beef extract peptone (BEP) medium and continuously stirred for 24 hours. The bacterial suspension was then diluted to a concentration of 1.0×10^5 colony-forming units (CFU)/mL. Next, 50 μL of the bacterial suspension was plated onto the surface of the samples. The samples, along with the bacteria on their surfaces, were co-incubated in darkness for 12 hours at a temperature of 37±0.5°C and a relative humidity exceeding 90%. After the incubation period, the samples were washed with sterilized PBS, and ultrasonic cleaning was performed to detach the bacteria from the samples. The samples were then sterilized and subjected to ultrasonic cleaning again before being re-incubated in 10 mL of sterilized PBS. This process was repeated for a duration of 28 days. Finally, the antibacterial activity at 1, 7, 14, 21, and 28 days was determined as previously reported in relevant studies.[17]

Inhibition Zone Method

Furthermore, the antibacterial performance of the samples was also analyzed using the inhibition zone method. Sterilized Petri dishes were filled with solid culture medium to a thickness of approximately 3 cm and allowed to solidify. Once the solid culture medium was set, 20 μL of bacterial suspension at a concentration of 1×10^8 CFU/mL was uniformly spread onto the surface of the sample. Simultaneously, the samples were inverted and placed in the center of the culture medium, ensuring full and effective contact between the samples and the medium. The Petri dishes were then incubated in a constant temperature incubator set to 37.0±0.5°C with humidity exceeding 90% for a period of 24 hours. After observing the size of the antibacterial zone, the samples were removed and reintroduced into fresh solid culture medium inoculated with new bacteria. This process was repeated for 28 days.

Ag Ions Release

The antibacterial activity of the samples was attributed to the precipitation of Ag ions. To investigate the pattern of Ag ions release, inductively coupled plasma mass spectrometry (ICPMS) was employed to measure the concentration of Ag ions in the leaching solution of the samples. Each group of samples was immersed in 10 mL sterile PBS solution. In order to simulate the post-implantation environment more accurately, we regularly replaced the PBS solution and conducted the soaking process in a constant temperature incubator set at 37.0±0.5°C. This process was carried out for a duration of 28 days. On the 1st, 7th, 14th, 21st, and 28th days, PBS leachates were collected and the Ag ion concentration in the leachate was measured using ICPMS.

Alkaline Phosphatase (ALP) Activity Assay

To quantitatively assess intracellular ALP activity, commercially available kits were utilized. Samples were placed into a 24-well plate and a 100 μL suspension of MC3T3-E1 cells at a density of 1×10^5 cells was seeded onto the sample surface. After co-incubation for 3 and 7 days, the cells were harvested. The Alkaline Phosphatase Assay Kit (Beyotime P0321M, China) was employed to measure ALP activity colorimetrically. Finally, the ALP activity was further normalized by total protein content, as previously described in relevant studies.[18]

Collagen Secretion Assay

Upon culturing for 7 and 14 days, a Sirius red staining-based colorimetric assay was performed to quantitatively measure collagen secretion from MC3T3-E1 cells on the samples. At the end of the induction period, the samples were rinsed with PBS and fixed with 75% ethanol for 1 hour. Following fixation, the cells were stained with 0.1 wt% Sirius Red dye at room temperature for 18 hours. Subsequently, the samples were thoroughly rinsed with deionized water until no excess dye residue remained. The cells were then washed with 1 mL of fading solution, which consisted of a 1:1 volume mixture of 99% methanol and 0.2 M NaOH solution. After allowing the solution to stand for 30 minutes, 150 μL of the eluent was transferred into a 96-well plate, and collagen secretion was quantitatively measured by determining the absorbance at 540 nm using a microplate reader (BioTek INstruments ELx800).

Extracellular Matrix Mineralization (ECM) Assay

Alizarin Red S staining (Sigma, USA) was utilized to assess the extent of ECM both qualitatively and quantitatively. Following co-incubation for 7 and 14 days, the samples were fixed with 75% ethanol for 1 hour. Next, the samples were washed with PBS and treated with 40 mm Alizarin Red S (pH 4.2) for 30 minutes at room temperature. Subsequently, the samples were rinsed with distilled water to remove any unbound stain completely. A fluorescence microscope from Olympus, Japan, was employed to observe the samples. Finally, 500 μL of a solution containing 10% cetylpyridinium chloride in 10 mm sodium phosphate buffer (pH 7.0) was used to elute the bound stain over a period of 2 hours. The absorbance of the 150 μL eluent was measured quantitatively at a wavelength of 620 nm using a microplate reader.

Quantitative Real-Time Polymerase Chain Reaction (qRT-PCR) Assay

To detect the mRNA expressions of osteogenesis-related genes, including ALP, bone morphogenic protein-2 (BMP-2), runt-related transcription factor 2 (RUNX2), and osteopontin (OPN), a qRT-PCR assay was performed. The samples were placed into a 6-well plate, and cells were seeded at a density of 1×10^5 cells per well. After incubation for 7 days, the cells were harvested, and total RNA was extracted using Trizol reagent (Invitrogen). Subsequently, a Prime Script RT reagent kit (Takara Bio Inc., Shiga, Japan) was utilized to reverse-transcribe 1μg of RNA into complementary DNA (cDNA). The expressions of the target genes were analyzed on the Bio-Rad C1000 system using SYBR Premix Ex Taq II (Takara). The relative expressions of the target genes were normalized using GAPDH (ab181602, Abcam) as the housekeeping gene. The primers used in this study are listed in Table 1.

Table 1 The Primers Used in qRT-PCR Assay

Sequence Name	Forward Primer (5′-3′)	Reverse Primer (5′-3′)
ALP	AACGTGGCCAAGAACATCATCA	TGTCCATCTCCAGCCGTGTC
BMP2	GAGAAGGAGGAGGCAAAGAAA	AGCAGCAACGCTAGAAGACAG
RUNX2	CCAACCCACGAATGCACTATC	TAGTGAGTGGCGGGACATAC
OPN	TCCTAGCCCCACAGACCCTT	CACACTATCACCTCGGCCAT
ERK5	GTGCCCTATGGCGAATTCAA	GCACGTGTTCCAGTGTGAGG
GAPDH	AGGGCTGCCTTCTCTTGTGA	AACTTGCCGTGGGTAGAGTCA

https://doi.org/10.2147/IJN.S493754

Western-Blot Array

The protein levels of osteogenesis-related proteins, including ALP (PA1004, Boster), BMP-2 (ab14933, Abcam), RUNX2 (ab114133, Abcam), and OPN (ab307994, Abcam), as well as the activity of extracellular signal-related kinases 5 (ERK5, ab196609, Abcam) signaling, were assessed using a Western blot array. Cells were seeded at a density of 1×10^5 cells per well in a 6-well plate and incubated for 24 hours. After incubation for 7 days, the cells were harvested. The protein levels were measured using the method described in the relevant literature.[19]

ERK5 Inhibition

The role of the ERK5 signaling pathway in osteogenesis promoted by silver ion-loaded titanium dioxide nanotube arrays was investigated by blocking ERK5. The titanium dioxide nanotube array was used as the control group, while the treatment group received a silver ion injection dosage of 1.0×10^{17} ions/cm^2 (based on preliminary experiments, this dosage showed the strongest stimulating effect on ERK5, whereas excessively high concentrations of silver ion injection had a certain inhibitory effect on bone integration). The treatment groups were divided into non-ERK5 inhibition group and ERK5 inhibition group, with the culture medium of the ERK5 inhibition group supplemented with a final concentration of 5μM of the specific ERK5 inhibitor, BIX02188 (S1530 Selleck, USA).

Statistical Analysis

After data collection, the data were analyzed by SPSS 23.0 statistical software, and the measurement data were expressed as mean±standard deviation. Following the descriptive statistics and a variance check (Levene's test), absorbance, antimicrobial rate as well as the relative expression of target genes and the ratio of target protein/internal reference protein optical density were analyzed by one-way ANOVA for between-group comparisons, and two-by-two comparisons were tested by Student-Newman-Keuls (SNK). The Fisher's LSD test was employed to ascertain the specific points of any discrepancies following the analysis. P-values less than 0.05 were considered significant.

Results

Sample Characterization

General Morphology of Samples

At first, the pure titanium foil exhibited a vibrant metallic hue. Nevertheless, the samples' color underwent a silver-gray transformation following anodic oxidation and Ag ion implantation, which progressively intensified as the Ag ion dosage increased. These alterations were observed in the titanium dioxide nanotube arrays that were laden with silver.

Microstructure of Samples

Structured titanium dioxide nanotubes were observed on the titanium foil's surface, as indicated by the scanning electron microscopy images. The nanotubes had a wall thickness of approximately 30 nm, a length of 5 μm, and a diameter of approximately 70 nm. The front view image demonstrates that the Ag ions are distributed in a sheet-like shape on the top surface of the titanium dioxide nanotubes when the Ag ions implantation dose is 5.0×10^{17} ions/cm^2. The surface of the titanium dioxide nanotube array is prominently covered with interconnected Ag ions. In contrast, for the doses of 1.0×10^{17} ions/cm^2 and 1.0×10^{18} ions/cm^2, the Ag ions exhibit a continuous grid structure with clustered aggregation on the surface of the titanium dioxide nanotubes, with differences observed in the size of the clusters. In comparison to the blank titanium dioxide nanotube array, the morphology of the titanium dioxide nanotube array exhibits varying degrees of injury following the implantation of Ag ions, as evidenced by the side view. This indicates that the nanotubes' structure may be subject to some physical harm as a result of the bombardment of Ag ions. Nevertheless, overall, the structure remains intact. Based on the bottom view results, the diameter and thickness of the lower half of the titanium dioxide nanotubes are relatively consistent. This indicates that the morphology and structure of the nanotubes may be slightly damaged by high-energy bombardment of Ag ions; However, this damage is primarily observed in the upper portion of the tubes and has a minimal impact on the lower half. Subsequent analysis utilizing HRTEM and EFTEM techniques demonstrated that Ag ions were uniformly distributed within the titanium dioxide nanotubes in all groups (Figure 1).

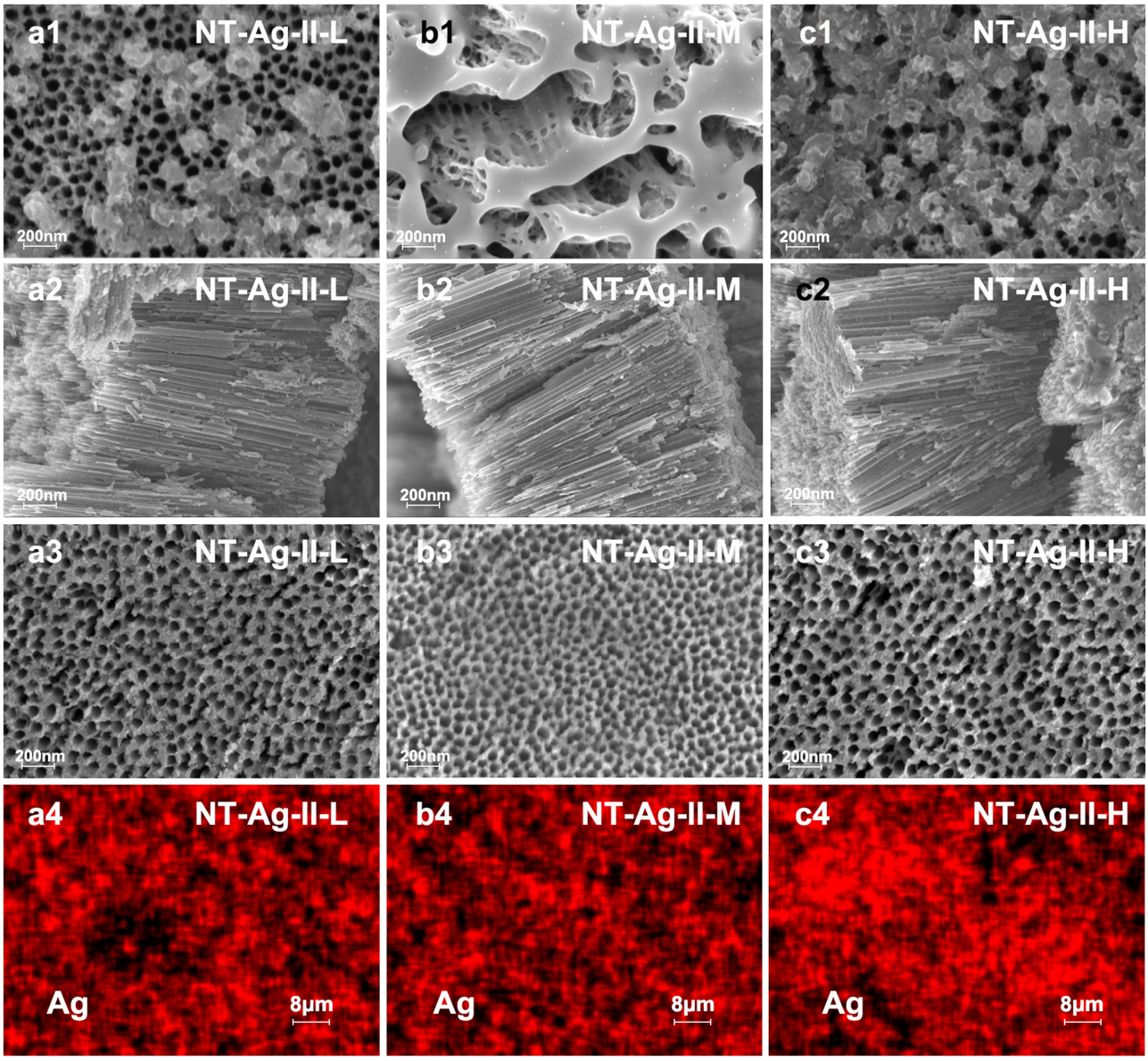

Figure 1 Scanning electron microscopy images (surface: **a1, b1, c1**, side: **a2, b2, c2**, and bottom: **a3, b3, c3**) and Ag ions distribution of titanium dioxide nanotube arrays with different Ag ions loading (**a4, b4, c4**).

Cell Proliferation

Cell proliferation was assessed to evaluate the cytocompatibility of the samples. The results, depicted in Figure 2, indicate that cell proliferation was similar across all groups. This suggests that there was no significant cytotoxicity introduced to the TiO_2 nanotubes by the Ag ions implantation process.

Cell Adhesion

To investigate the initial adhesion and spreading behavior of MC3T3-E1 cells, rhodamine phalloidin and DAPI staining were employed to visualize the cytoskeleton of the co-cultured cells. As illustrated in Figure 2, the majority of cells on the samples exhibited a spherical morphology with intense expression of F-actin. However, cells on the NT-Ag-II-M group showed better spreading compared to other groups. These findings suggest that the Ag ions implantation, particularly in the NT-Ag-II-M group, could enhance the initial adhesion and spreading activity of MC3T3-E1 cells.

https://doi.org/10.2147/IJN.S493754

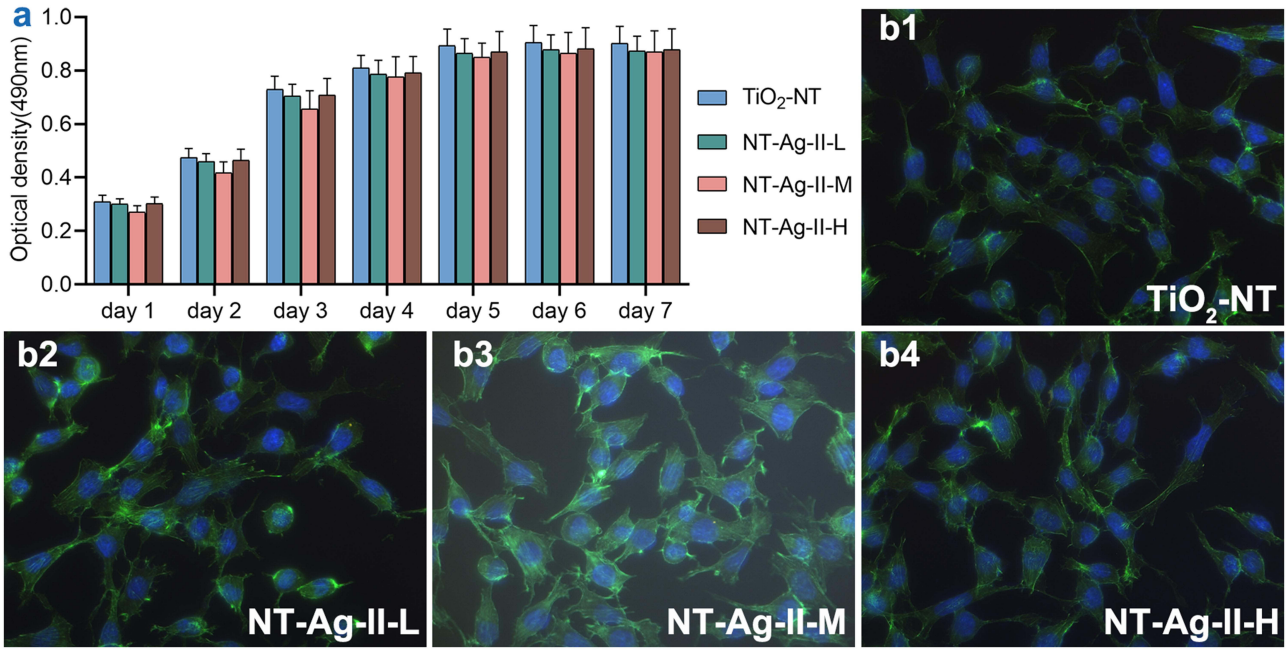

Figure 2 Proliferation and cytoskeletal staining plots of mouse MC3T3-E1 cells cultured on the surface of titanium dioxide nanotube arrays (**a**) and titanium dioxide nanotube arrays with different Ag ions loading (**b1**–**b4**) (×200). Data are expressed as mean ± SD. N=3.

Antibacterial Property

Plate-Counting Method

Figure 3 illustrates the antibacterial performance of the samples against suspended bacteria. The results demonstrate excellent antibacterial efficacy in the first 7 days, followed by a noticeable decline thereafter. By the 28th day, the antibacterial rates for S. aureus were 50.61% for NT-Ag-II-L, 70.86% for NT-Ag-II-M, and 75.11% for NT-Ag-II-H. Regarding E. coli, the antibacterial rates were 60.22% for NT-Ag-II-L, 77.23% for NT-Ag-II-M, and 83.47% for NT-Ag-II-H. Notably, the NT-Ag-II-L group, with a lower Ag implantation, exhibited a more rapid decrease in antibacterial activity over time. Conversely, there was no significant differences in the antibacterial rate between the NT-Ag-II-M and NT-Ag-II-H groups.

Inhibition Zone Method

The inhibition zone method was employed to further validate the long-term antibacterial activity of the samples against S. aureus and E. coli adhering to their surfaces. As depicted in Figure 3, the control group, which lacked Ag implantation, was unable to form a bacteriostatic ring. In contrast, the other groups exhibited significant bacteriostatic rings, with the NT-Ag-II-H group displaying the largest bacteriostatic ring among them. These results confirm the excellent long-term antibacterial activity of the samples, with the NT-Ag-II-H group demonstrating the highest efficacy.

The Release of Ag Ions

To further investigate the mechanism behind the antibacterial performance of silver-loaded titanium dioxide nanotube arrays, the leaching solution from the samples was analyzed using ICPMS to measure the concentration of Ag ions. As depicted in Figure 3, the overall trend shows a gradual decrease in the release of Ag ions over time, particularly within the first 14 days. After this initial period, the amount of Ag ions release tends to stabilize. Initially, the NT-Ag-II-M group exhibited the highest Ag ions concentration in the leachate, followed by the NT-Ag-II-H group and NT-Ag-II-L group. This could be attributed to the sheet-like distribution of Ag ions on the surface of the titanium dioxide nanotube array in the NT-Ag-II-M group, creating a larger contact area with the surrounding solution. However, as time progresses, the amount of Ag ions precipitation gradually reached a stable state, and the concentration of Ag ions in the leachate after 14 days became significantly related to the dose of Ag ions implanted into the sample.

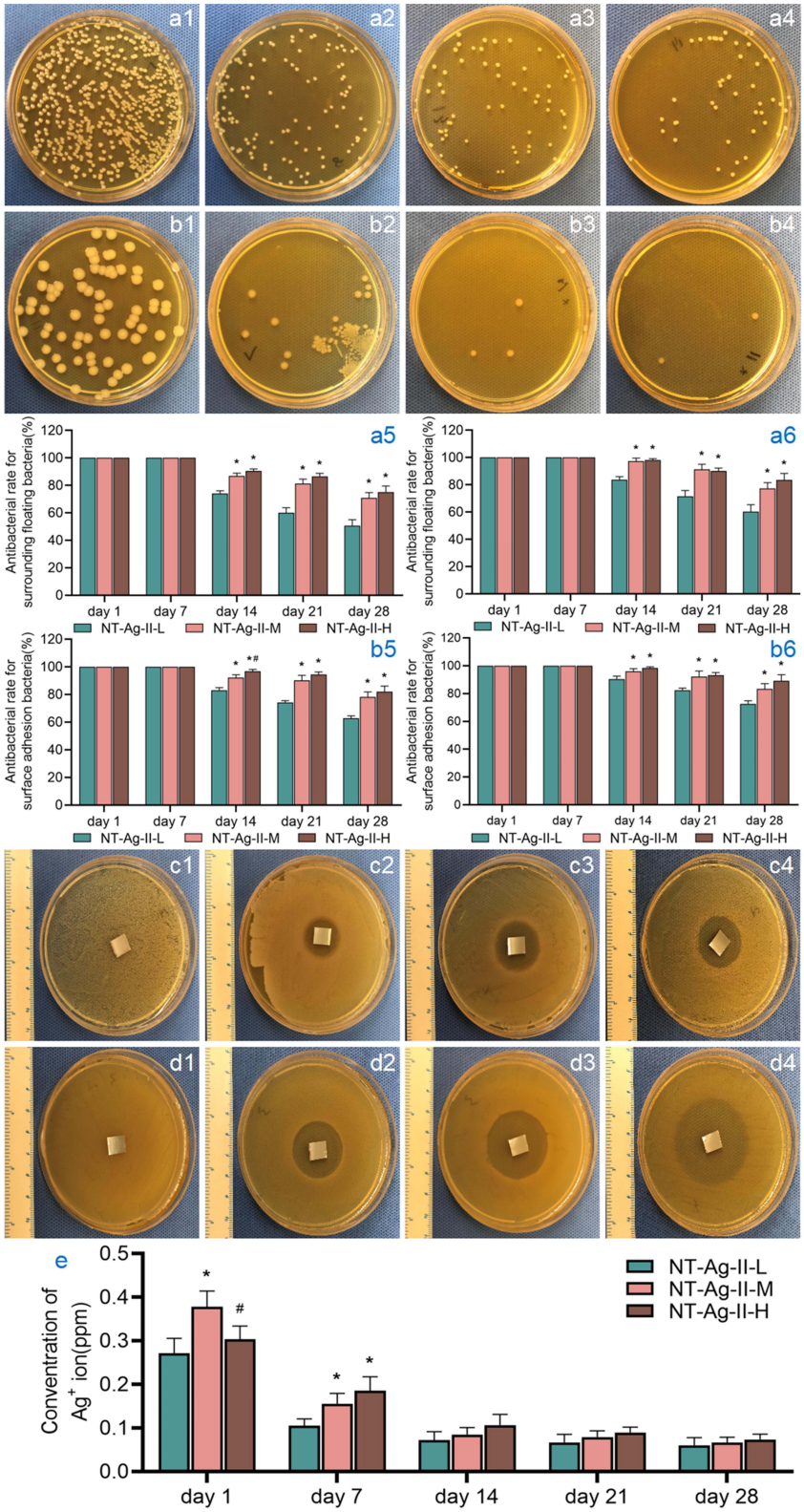

Figure 3 Bacterial colony counting in eluate culture on day 28 of titanium dioxide nanotube array and different silver-loaded titanium dioxide nanotube array ((**a1**–**a4**) S. aureus; (**b1**–**b4**) E. coli). Bacterial inhibition rate of titanium dioxide nanotube array and different silver-loaded titanium dioxide nanotube arrays against suspended ((**a5**) S. aureus; (**b5**) E. coli) and adherent ((**a6**) S. aureus; (**b6**) E. coli) bacteria on day 1/7/14/21/28. Observation of bacterial inhibitory ring on day 28 of titanium dioxide nanotube array and different silver-loaded titanium dioxide nanotube arrays ((**c1**–**c4**) S. aureus; (**d1**–**d4**) E. coli); Non-accumulative Ag ions concentrations in immersion solutions of silver-loaded titanium dioxide nanotube arrays are shown in (**e**). Data are expressed as mean ± SD. *P<0.05, compared with TiO_2 NT group. #P<0.05, compared with NT-Ag-II-L group. N=3.

https://doi.org/10.2147/IJN.S493754

Osteoblastic Differentiation

The osteoblastic differentiation of MC3T3-E1 cells in different groups was assessed by measuring ALP production, collagen secretion, and ECM. As shown in Figure 4, compared to the 3-day induction period, ALP production significantly increased in all groups after 7 days of induction. However, there was no significant difference observed among the four groups after the 7-day induction period. The collagen secretion of MC3T3-E1 cells was also measured after co-incubation for 7 and 14 days, as shown in Figure 4. After 7 days, the TiO_2-NT group and NT-Ag-II-L group exhibited higher collagen secretion compared to the NT-Ag-II-M and NT-Ag-II-H groups. However, this difference diminished after incubation for 14 days, except for the NT-Ag-II-H group. The results of ECM were similar to the collagen secretion findings, as depicted in Figure 4.

The results depicted in Figure 5 suggest that the improvement in the osteogenic performance of silver-loaded titanium dioxide nanotube arrays may be attributed to the activation of the ERK5 signal by Ag ions.

qRT-PCR Assays and Western Blot Assays

The osteoblastic differentiation of MC3T3-E1 cells in different groups was further assessed using qRT-PCR assays and Western blot assays (Figure 6). Overall, after 7 days of induction, the mRNA expressions and protein levels of ALP, BMP-2, RUNX2, and OPN in MC3T3-E1 cells on the surface of silver-loaded titanium dioxide nanotube arrays were found to increase. Moreover, as the dosage of Ag ions increased, the mRNA expression and protein levels of these markers also gradually increased, with the NT-Ag-II-H group exhibiting the highest levels among the groups.

In addition, qRT-PCR assays and Western blot assays were conducted to examine the activity of ERK5 signaling, a key factor in osteogenic regulation.[20,21] The results depicted in Figure 6 demonstrate that Ag ions implantation can significantly enhance the mRNA expression and protein levels of ERK5, particularly in the NT-Ag-II-M group. When the activity of ERK5 was suppressed, there was a significant decrease in the mRNA expressions and protein levels of ALP, BMP-2, RUNX2, and OPN in MC3T3-E1 cells on the surface of the samples (Figure 7).

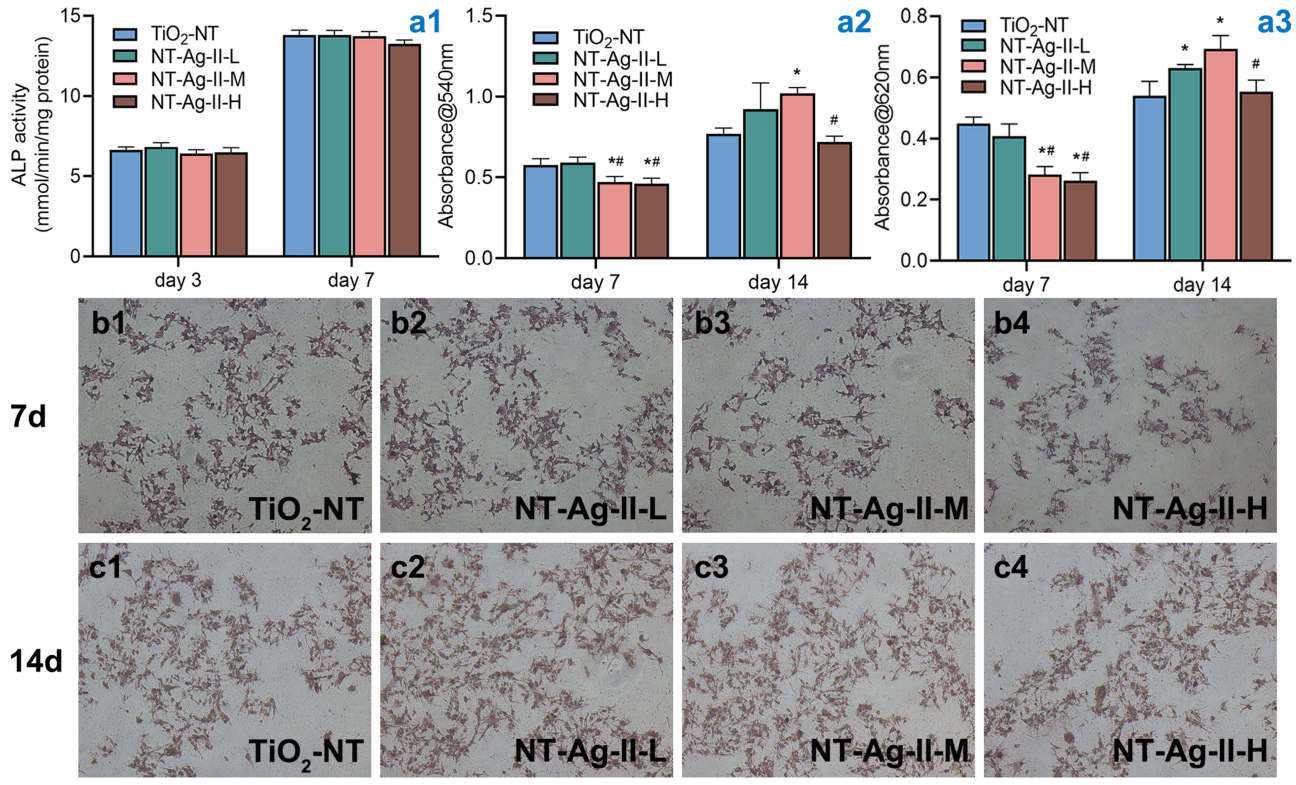

Figure 4 Osteogenic activity of MC3T3-E1 cells on the surface of titanium dioxide nanotube arrays and silver-loaded titanium dioxide nanotube arrays after induction and differentiation ((**a1**) ALP; (**a2**) Collagen; (**a3**) ECM); Alizarin red stained image of MC3T3-E1 cells on the surface of titanium dioxide nanotube arrays and different silver-loaded titanium dioxide nanotube arrays after 7 (**b1–b4**) and 14 days (**c1–c4**) of induced differentiation (×40). Data are expressed as mean ± SD. *P<0.05, compared with TiO_2 NT group. #P<0.05, compared with NT-Ag-II-L group. N=3.

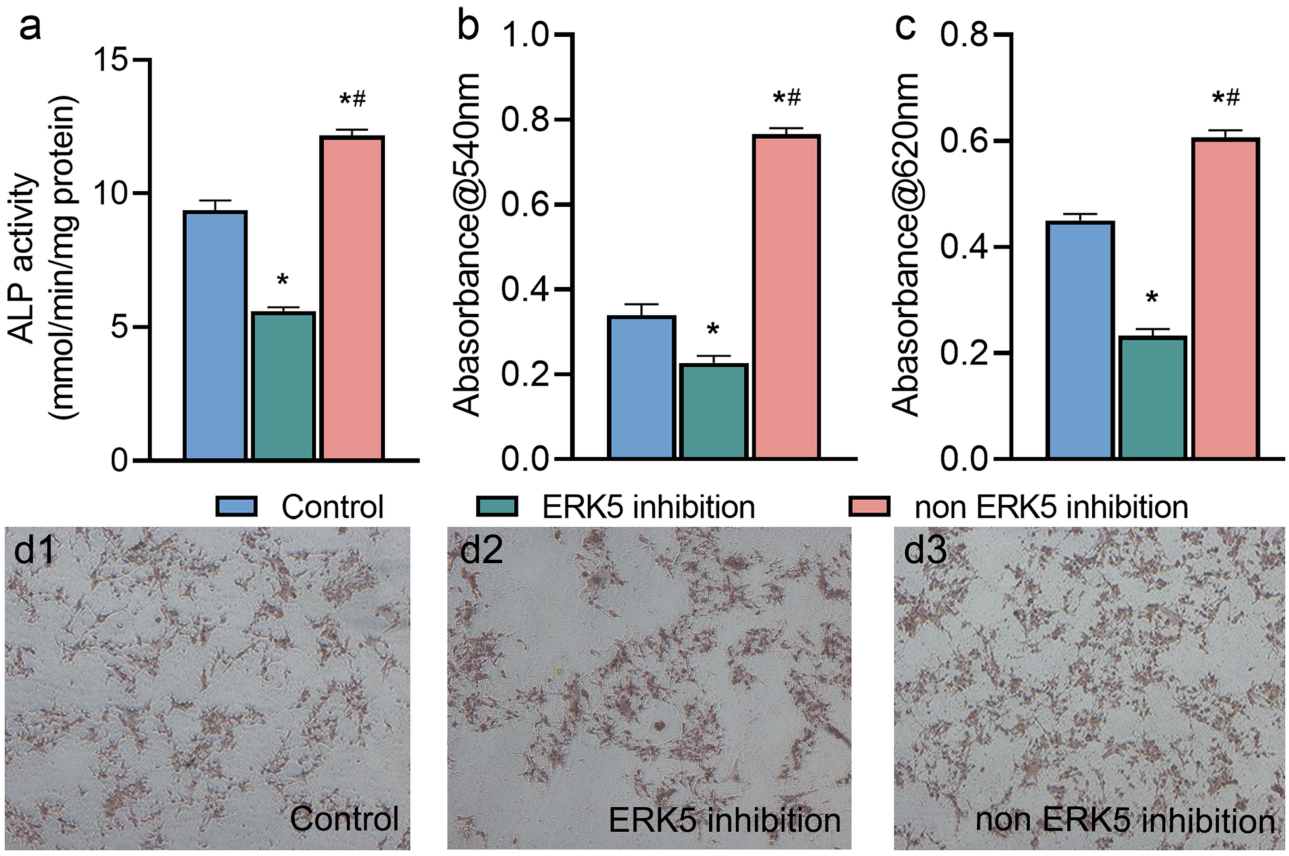

Figure 5 Osteogenic activity of MC3T3-E1 cells on the surface of different groups after induction and differentiation ((**a**) ALP; (**b**) Collagen; (**c**) ECM); Alizarin red stained image of MC3T3-E1 cells on the surface of different groups after induction and differentiation (**d1**–**d3**) (×40). Data are expressed as mean ± SD. *P<0.05, compared with Control group. #P<0.05, compared with ERK5 inhibition group.N=3.

Discussion

Infection and implant loosening are significant complications following internal fixation surgery.[22,23] Surface modification techniques offer an effective solution for metallic implants by enhancing their antimicrobial properties and promoting bone integration.[24,25] Considering that implant-related infections can occur long after surgery, the development of surface modification techniques that enable sustained release of antimicrobial agents and maintain long-term stability is particularly crucial.[26,27] Due to the improper use of antibiotics, the problem of bacterial resistance to antibiotics is becoming increasingly severe. Inorganic antibacterial agents, including metal elements such as silver, copper, and zinc, are an important supplement to antibiotics.[28] In previous studies, there have been many reports on the application of heavy metal ions in antibacterial materials. However, silver ions have shown significant advantages in the field of antibacterial materials due to their broad-spectrum, high-efficiency antibacterial properties, low toxicity, safety, and diverse antibacterial mechanisms.[29,30] Firstly, silver ions exhibit strong antibacterial activity against both Gram positive and Gram negative bacteria, and compared to other metal antibacterial materials, their antibacterial effect is more significant, making it less likely to induce bacterial resistance. Secondly, silver ions have relatively low toxicity to human cells at effective antibacterial concentrations, making their application in the medical field and daily necessities safer. Finally, silver ions exert antibacterial effects by disrupting various mechanisms such as bacterial cell walls, cell membranes, respiratory chains, and DNA, while nano silver particles further enhance the antibacterial effect of silver ions due to their enhanced permeability. These characteristics collectively establish the important role of silver ions in applications that require efficient, safe, and long-lasting antibacterial effects.[30,31] Ag ions serve as commonly used inorganic antimicrobial agents, while TiO_2 nanotubes have demonstrated improved biocompatibility and osseointegration abilities for titanium implants.[12,13,32,33] Additionally, TiO_2 nanotubes possess a high specific surface area, making them

https://doi.org/10.2147/IJN.S493754

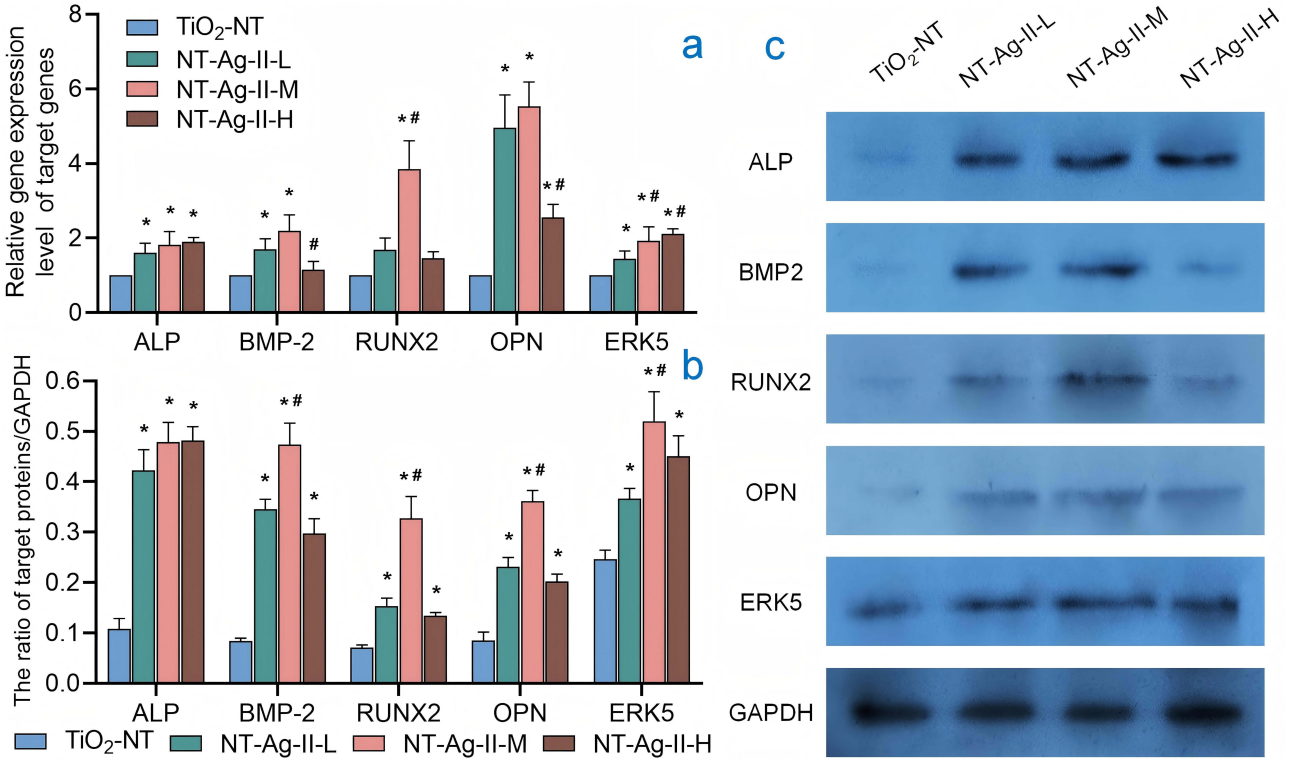

Figure 6 Gene transcription (**a**) and protein expression (**b** and **c**) levels of osteogenesis-related factor of MC3T3-E1 cells on titanium dioxide nanotube arrays and different silver-loaded titanium dioxide nanotube arrays after 7 days of induced differentiation. Data are expressed as mean ± SD. *P<0.05, compared with TiO_2 NT group. #P<0.05, compared with NT-Ag-II-L group. N=3.

ideal carriers for drug delivery.[34] There are various silver ion loading technologies, each with its own advantages, and ion implantation is just one of them. However, the ion implantation method stands out due to its precise control of doping depth and concentration, low-temperature process, and reliable combination. The ion implantation method can accurately control the depth and concentration of the doping layer, which is crucial for surface modification of materials. Meanwhile, this method is carried out at lower temperatures, reducing the potential material damage that may occur during the heat treatment process. In addition, ion implantation technology also facilitates the binding of silver ions on the substrate surface, slowing down the release rate of silver ions, thereby achieving sustained release of silver ions and improving their biological safety.[35,36] This study utilized anodization and ion implantation to combine the antimicrobial properties of Ag ions with the bone-promoting capabilities of TiO_2 nanotubes, resulting in the development of a novel surface modification method for titanium metal. This approach enhanced the antimicrobial efficacy and osteogenic ability of the implant material.

Scanning electron microscopy revealed that anodization and metal vapor vacuum arc implantation of Ag ions successfully constructed titanium dioxide nanotube arrays laden with Ag ions on the titanium surface. However, it is important to note that ion implantation may cause structural damage to the titanium dioxide nanotubes, emphasizing the need for appropriate dosage selection when loading Ag ions into the nanotube array. Based on this study's findings, we recommend limiting the loading of Ag ions to not exceed 1.0×10^{18} ions/cm^2.

Biocompatibility serves as a crucial indicator for evaluating implants. MTT experiments indicated that Ag ion implantation does not significantly increase the biotoxicity of titanium dioxide nanotubes. On the contrary, the inclusion of a small amount of Ag ions promotes early osteoblast adhesion, potentially due to the positive regulatory effect of low Ag ions concentrations on cell growth.[37,38] In this study, we investigated the relationship between the antibacterial performance of silver loaded coatings and their silver ion release. Research has shown that surface coatings that continuously release silver ions have corresponding bactericidal effects. However, due to the potential toxicity of silver ions to human tissues at high concentrations (with a minimum bactericidal concentration of 0.1 ppm and a cytotoxic

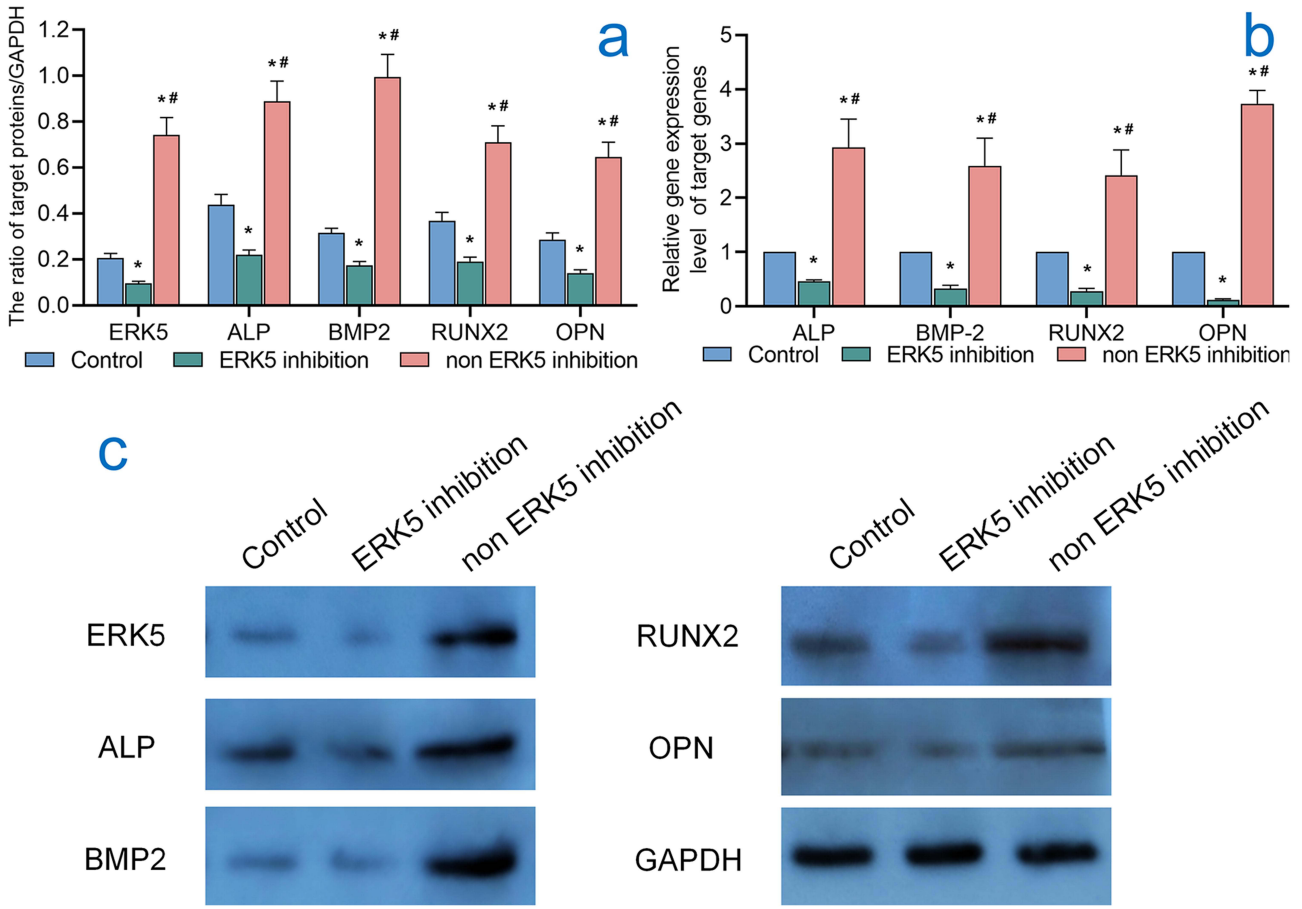

Figure 7 Gene transcription (**a**) and protein expression (**b** and **c**) levels of osteogenesis-related factor of MC3T3-E1 cells in different groups after induced differentiation. Data are expressed as mean ± SD. *P<0.05, compared with Control group. #P<0.05, compared with ERK5 inhibition group. N=3.

concentration of 1.6 ppm), the release concentration of silver ions must be strictly controlled to avoid damage to human cells.[39] Although some studies have suggested that cytotoxicity only occurs when the concentration of silver ions exceeds 2 ppm, and apoptosis of mouse spermatogonial stem cells is only induced when the concentration of nano silver reaches 5–10 ppm.[35,39] This study detected the release of silver ions from silver loaded samples using an inductively coupled plasma mass spectrometer. The results showed that all silver loaded samples released a large amount of silver ions within the first 14 days, with a maximum release of 0.3033 ppm. After that, the release gradually decreased and tended to stabilize. Within 28 days, the cumulative release of silver ions in 10 mL PBS remained between 0.5767 ppm and 0.7590 ppm, with a total release of 7.59μg. For example, with a standard size plate (10cm×2cm×0.5 cm, 52 cm^2), the highest silver release within 28 days was 394.68μg. Considering that the adult human body fluid volume is approximately 40 L, when silver ions are evenly distributed in the body fluid, their concentration is below the safe concentration threshold.[40] Therefore, the release amount of the samples in PBS in this study can maintain the effective bactericidal concentration while being lower than the cytotoxic concentration.

Antimicrobial assay results indicate that silver-loaded titanium dioxide nanotube arrays have long-lasting antimicrobial effects against common clinical pathogens, including Gram-positive bacterium Staphylococcus aureus and Gram-negative bacterium Escherichia coli. Particularly, the early antimicrobial effect is notably pronounced, which holds promising implications for clinical applications since the early stage after internal fixation surgery carries a higher risk of infection.[41] In conjunction with the Ag ions release test, it is evident that Ag ions release from the silver-loaded titanium dioxide nanotube arrays is not significant. This limited release can be attributed to the strong bonding between the Ag ions and the substrate, resulting from high-energy implantation. Additionally, different metals possess varying corrosion potentials, with the titanium-silver alloy experiencing more corrosion on the titanium metal side and less on the silver side when exposed to

physiological environments.[42,43] Consequently, this differential corrosion leads to a lower release of Ag ions, potentially explaining the absence of significant cytotoxicity even with a higher dosage of loaded Ag ions. Moreover, the antimicrobial efficacy results demonstrate that the silver-loaded titanium dioxide nanotube arrays exhibit antimicrobial effects not only through the direct release of Ag ions but also via direct contact, effectively killing bacteria adhered to their surface. Furthermore, the Ag ions elution experiment suggests the involvement of additional mechanisms in the antimicrobial activity of the samples, beyond the direct bactericidal effect of Ag ions. When the titanium-silver alloy interacts with physiological environments, a micro-galvanic corrosion arises between titanium and silver. This effect disrupts the distribution of protons and electrons, leading to ATP consumption through proton transmembrane transport in bacteria, ultimately disrupting bacterial energy metabolism and transportation processes.[44–46] These combined effects contribute to the antimicrobial properties observed.

ERK5, as an atypical member of the MAPK family, plays a regulatory role in osteogenic-related factors such as ALP, BMP2, RUNX2, and OPN, consequently influencing the biological functions of osteoblasts.[18,21,47] Previous studies have found that silver ions may trigger a series of phosphorylation cascades by interacting with cell surface receptors, thereby activating the ERK5 signaling pathway. Specifically, silver ions may promote the activation of MEK5 (an upstream kinase of ERK5), leading to phosphorylation and nuclear translocation of ERK5, ultimately regulating the expression of downstream genes, including transcription factors and cell cycle proteins related to osteogenic differentiation. Research findings suggest that Ag ions loaded onto the surface of titanium dioxide nanotube arrays enhance both the transcriptional expression and protein levels of ERK5 in array surface osteoblasts. However, this positive effect may plateau after surpassing a certain concentration ($\geq 1.0\times10^{18}$ ions/cm^2) of Ag ions. Additionally, ERK5 mediates the bone integration effects of silver-loaded titanium dioxide nanotube arrays by regulating downstream osteogenic-related factors such as ALP, BMP2, RUNX2, and OPN.

This study has achieved preliminary results in exploring the antibacterial performance and bone integration ability of silver ion loaded titanium dioxide nano coatings, but there are still several limitations. Firstly, due to resource limitations, this study was limited to in vitro experiments and lasted for 28 days, and was unable to validate the antibacterial effect, bone integration potential, and biocompatibility of the coating in longer cycles and animal models. Secondly, although preliminary discussions have been conducted on the antibacterial and bone promoting mechanisms of coatings, there is still a lack of in-depth understanding of the specific details of these mechanisms, and further research is needed on the mechanism of the interaction between the long-term antibacterial effect of silver ion release and bone formation. Finally, this study focuses on the biological functions of coatings, while the adhesion strength on titanium metal surfaces and stability during production and transportation have not been thoroughly explored. These aspects urgently need to be addressed in our future research.

Conclusion

In conclusion, the combination of anodic oxidation and metal vapor vacuum arc implantation of Ag ions effectively enhanced the antibacterial activity of titanium. Additionally, it improved the adhesion, proliferation, and osteogenic differentiation of MC3T3-E1 cells on the silver-loaded titanium dioxide nanotube arrays. This research demonstrates the potential of this surface modification technique for developing implantable materials with enhanced antibacterial properties and improved osteogenesis effect.

The Translational Potential of This Article

The results of this study indicate a simple and stable surface modification method for titanium metal, which combines the antimicrobial effect of silver ions with the osteogenic properties and drug carrier functionality of titanium dioxide nanotubes. This method holds promising prospects for applications in constructing silver-loaded titanium dioxide nanotube arrays on the surface of titanium implants, which not only endows the titanium implants with long-lasting antimicrobial properties but also enhances their osteogenic performance.

Journalism Ethics Considerations

Ethical issues (Including plagiarism, Informed Consent, misconduct, data fabrication and/or falsification, double publication and/or submission, redundancy, etc.) have been completely observed by the authors.

Acknowledgments

The project was supported by 2024 Guangzhou Municipal Science and Technology Bureau City-University Collaboration Project (2024A03J0664), Guangzhou Key Disciplines in Medical Sciences Project (2025-2027) and 2017 Guangzhou Medical and Health Science and Technology Project (20171A011252).

Disclosure

The authors declare that there is no conflict of interest.

References

1. Yayac M, Trojan JD, Brown S, Mulcahey MK. Formal leadership training for orthopedic surgeons: limited opportunities amongst growing demand. *Orthop Rev*. 2019;11(4):8151. doi:10.4081/or.2019.8151
2. Ghilini F, Fagali N, Pissinis DE, Benitez G, Schilardi PL. Multifunctional titanium surfaces for orthopedic implants: antimicrobial activity and enhanced osseointegration. *ACS Appl Bio Mater*. 2021;4(8):6451–6461. doi:10.1021/acsabm.1c00613
3. Muhlhofer HML, Feihl S, Suren C, Banke IGJ, Pohlig F, von Eisenhart-Rothe R. Implantatassoziierte Gelenkinfektionen [Implant-associated joint infections]. *Orthopade*. 2020;49(3):277–286. doi:10.1007/s00132-020-03877-w
4. Dapunt U, Prior B, Kretzer JP, Hansch GM, Gaida MM. The effect of surgical suture material on osteoclast generation and implant-loosening. *Int J Med Sci*. 2021;18(2):295–303. doi:10.7150/ijms.50270
5. Wang X, Ning B, Pei X. Tantalum and its derivatives in orthopedic and dental implants: osteogenesis and antibacterial properties. *Colloids Surf B Biointerfaces*. 2021;208:112055. doi:10.1016/j.colsurfb.2021.112055
6. Jia F, Guan J, Wang J, et al. Zinc and melatonin mediated antimicrobial, anti-inflammatory, and antioxidant coatings accelerate bone defect repair. *Colloids Surf B*. 2025;245:114335. doi:10.1016/j.colsurfb.2024.114335
7. Jia F, Xu D, Sun Y, et al. Strontium-calcium doped titanium dioxide nanotubes loaded with GL13K for promotion of antibacterial activity, anti-inflammation, and vascularized bone regeneration. *Ceram Int*. 2023;49(22, Part B):35703–35721. doi:10.1016/j.ceramint.2023.08.250
8. Kunrath MF, Farina G, Sturmer LBS, Teixeira ER. TiO(2) nanotubes as an antibacterial nanotextured surface for dental implants: systematic review and meta-analysis. *Dent Mater*. 2024;40(6):907–920. doi:10.1016/j.dental.2024.04.009
9. Jafari S, Mahyad B, Hashemzadeh H, Janfaza S, Gholikhani T, Tayebi L. Biomedical applications of TiO(2) nanostructures: recent advances. *Int J Nanomed*. 2020;15:3447–3470. doi:10.2147/IJN.S249441
10. Jiang N, Chen L, Ma Q, Ruan J. Nanostructured Ti surfaces and retinoic acid/dexamethasone present a spatial framework for the maturation and amelogenesis of LS-8 cells. *Int J Nanomed*. 2018;13:3949–3964. doi:10.2147/IJN.S167629
11. Wang K, Jin H, Song Q, Huo J, Zhang J, Li P. Titanium dioxide nanotubes as drug carriers for infection control and osteogenesis of bone implants. *Drug Deliv Transl Res*. 2021;11(4):1456–1474. doi:10.1007/s13346-021-00980-z
12. Ocampo RA, Echeverria FE. Antibacterial and biological behavior of TiO2 nanotubes produced by anodizing technique. *Crit Rev Biomed Eng*. 2021;49(1):51–65. doi:10.1615/CritRevBiomedEng.2021037758
13. Xu L, Wang YY, Huang J, Chen CY, Wang ZX, Xie H. Silver nanoparticles: synthesis, medical applications and biosafety. *Theranostics*. 2020;10(20):8996–9031. doi:10.7150/thno.45413
14. Zhang Y, Sun N, Hu F, et al. Combined release of LL37 peptide and zinc ion from a mussel-inspired coating on porous titanium for infected bone defect repairing. *Colloids Surf B*. 2024;244:114181. doi:10.1016/j.colsurfb.2024.114181
15. Rautray TR, Narayanan R, Kwon TY, Kim KH. Surface modification of titanium and titanium alloys by ion implantation. *J Biomed Mater Res B Appl Biomater*. 2010;93(2):581–591. doi:10.1002/jbm.b.31596
16. Swain S, Pradhan M, Bhuyan S, Misra RDK, Rautray TR. On the ion implantation synthesis of Ag-embedded over Sr-substituted hydroxyapatite on a nano-topography patterned Ti for application in acetabular fracture sites. *Int J Nanomed*. 2024;19:4515–4531. doi:10.2147/IJN.S464905
17. Jiang L, Zhang B, Liu S, Zhu L, Zhu F. The MBS microbial rapid detection system for rapid detection of major pathogenic bacteria in feed: comparison with plate counting method. *BMC Microbiol*. 2022;22(1):242. doi:10.1186/s12866-022-02655-2
18. He J, Wang X, Zhao D, Geng B, Xia Y. Mangiferin promotes osteogenic differentiation and alleviates osteoporosis in the ovariectomized mouse via the AXL/ERK5 pathway. *Front Pharmacol*. 2022;13:1028932. doi:10.3389/fphar.2022.1028932
19. Sun B, Wu H, Lu J, et al. Irisin reduces bone fracture by facilitating osteogenesis and antagonizing TGF-beta/Smad signaling in a growing mouse model of osteogenesis imperfecta. *J Orthop Translat*. 2023;38:175–189. doi:10.1016/j.jot.2022.10.012
20. Wen L, Liu Z, Zhou L, et al. Bone and Extracellular Signal-Related Kinase 5 (ERK5). *Biomolecules*. 2024;14(5):556. doi:10.3390/biom14050556
21. Horie T, Fukasawa K, Yamada T, et al. Erk5 in bone marrow mesenchymal stem cells regulates bone homeostasis by preventing osteogenesis in adulthood. *Stem Cells*. 2022;40(4):411–422. doi:10.1093/stmcls/sxac011
22. Liu Y, Du T, Qiao A, Mu Y, Yang H. Zinc-based biodegradable materials for orthopaedic internal fixation. *J Funct Biomater*. 2022;13(4):164. doi:10.3390/jfb13040164
23. Ma QL, Fang L, Jiang N, et al. Bone mesenchymal stem cell secretion of sRANKL/OPG/M-CSF in response to macrophage-mediated inflammatory response influences osteogenesis on nanostructured Ti surfaces. *Biomaterials*. 2018;154:234–247. doi:10.1016/j.biomaterials.2017.11.003
24. Gao S, Lu R, Wang X, et al. Immune response of macrophages on super-hydrophilic TiO(2) nanotube arrays. *J Biomater Appl*. 2020;34(9):1239–1253. doi:10.1177/0885328220903249
25. Cowden K, Dias-Netipanyj MF, Popat KC. Adhesion and proliferation of human adipose-derived stem cells on titania nanotube surfaces. *Regen Eng Transl Med*. 2019;5(4):435–445. doi:10.1007/s40883-019-00091-9
26. Mori Y, Masahashi N, Aizawa T. A review of anodized TiNbSn alloys for improvement in layer quality and application to orthopedic implants. *Materials*. 2022;15(15):5116. doi:10.3390/ma15155116
27. Li J, Fan Z, Huang M, Xie Y, Guan Z, Ruan J. Enhanced healing process of tooth sockets using strontium-doped TiO(2). *RSC Adv*. 2022;12(28):17817–17820. doi:10.1039/d2ra00341d

28. Hang R, Gao A, Huang X, et al. Antibacterial activity and cytocompatibility of Cu-Ti-O nanotubes. *J Biomed Mater Res A*. 2014;102 (6):1850–1858. doi:10.1002/jbm.a.34847
29. Pires LA, de Azevedo Silva LJ, Ferrairo BM, et al. Effects of ZnO/TiO(2) nanoparticle and TiO(2) nanotube additions to dense polycrystalline hydroxyapatite bioceramic from bovine bones. *Dent Mater*. 2020;36(2):e38–e46. doi:10.1016/j.dental.2019.11.006
30. Liu M, Wu K, Zhao L, Zhang Y. Foreign body reaction to biomaterial nanotubular surface and the influence of silver loading. *J Biomed Nanotechnol*. 2017;13(4):381–392. doi:10.1166/jbn.2017.2354
31. Chen J, Mei ML, Li Q, Chu C-H. Mussel-inspired silver-nanoparticle coating on porous titanium surfaces to promote mineralization. *RSC Adv*. 2016;6:104025–104035. doi:10.1039/C6RA20673E
32. Jia X, Wang L, Chen Y, et al. TiO(2)nanotubes induce early mitochondrial fission in BMMSCs and promote osseointegration. *Biomed Mater*. 2023;18(2):025008. doi:10.1088/1748-605X/acb7bc
33. Malec K, Goralska J, Hubalewska-Mazgaj M, et al. Effects of nanoporous anodic titanium oxide on human adipose derived stem cells. *Int J Nanomed*. 2016;11:5349–5360. doi:10.2147/IJN.S116263
34. Miyabe S, Fujinaga Y, Tsuchiya H, Fujimoto S. TiO(2) nanotubes with customized diameters for local drug delivery systems. *J Biomed Mater Res B Appl Biomater*. 2024;112(7):e35445. doi:10.1002/jbm.b.35445
35. Mei S, Wang H, Wang W, et al. Antibacterial effects and biocompatibility of titanium surfaces with graded silver incorporation in titania nanotubes. *Biomaterials*. 2014;35(14):4255–4265. doi:10.1016/j.biomaterials.2014.02.005
36. Allen FI. A review of defect engineering, ion implantation, and nanofabrication using the helium ion microscope. *Beilstein J Nanotechnol*. 2021;12:633–664. doi:10.3762/bjnano.12.52
37. Sivaraj D, Vijayalakshmi K. Enhanced antibacterial and corrosion resistance properties of Ag substituted hydroxyapatite/functionalized multiwall carbon nanotube nanocomposite coating on 316L stainless steel for biomedical application. *Ultrason Sonochem*. 2019;59:104730. doi:10.1016/j.ultsonch.2019.104730
38. Han X, Ma J, Tian A, et al. Surface modification techniques of titanium and titanium alloys for biomedical orthopaedics applications: a review. *Colloids Surf B Biointerfaces*. 2023;227:113339. doi:10.1016/j.colsurfb.2023.113339
39. Roy P, Berger S, Schmuki P. TiO2 nanotubes: synthesis and applications. *Angew Chem Int Ed Engl*. 2011;50(13):2904–2939. doi:10.1002/anie.201001374
40. Zhang L, Zhang L, Yang Y, et al. Inhibitory effect of super-hydrophobicity on silver release and antibacterial properties of super-hydrophobic Ag/TiO2 nanotubes. *J Biomed Mater Res B Appl Biomater*. 2016;104(5):1004–1012. doi:10.1002/jbm.b.33454
41. Han SH, Park JS, Baek JH, Kim S, Ku KH. Complications associated with open reduction and internal fixation for adult distal humerus fractures: a multicenter retrospective study. *J Orthop Surg Res*. 2022;17(1):399. doi:10.1186/s13018-022-03292-1
42. Kang DK, Moon SK, Oh KT, Choi GS, Kim KN. Properties of experimental titanium-silver-copper alloys for dental applications. *J Biomed Mater Res B Appl Biomater*. 2009;90(1):446–451. doi:10.1002/jbm.b.31305
43. Pawlowski L, Rosciszewska M, Majkowska-Marzec B, et al. Influence of surface modification of titanium and its alloys for medical implants on their corrosion behavior. *Materials*. 2022;15(21):7556. doi:10.3390/ma15217556
44. Jin G, Qin H, Cao H, et al. Zn/Ag micro-galvanic couples formed on titanium and osseointegration effects in the presence of S. aureus. *Biomaterials*. 2015;65:22–31. doi:10.1016/j.biomaterials.2015.06.040
45. Tan L, Hu Y, Hou Y, et al. Osteogenic differentiation of mesenchymal stem cells by silica/calcium micro-galvanic effects on the titanium surface. *J Mater Chem B*. 2020;8(11):2286–2295. doi:10.1039/d0tb00054j
46. Cao H, Liu X, Meng F, Chu PK. Biological actions of silver nanoparticles embedded in titanium controlled by micro-galvanic effects. *Biomaterials*. 2011;32(3):693–705. doi:10.1016/j.biomaterials.2010.09.066
47. Guo TM, Xing YL, Zhu HY, Yang L, Liu GX, Qiao XM. Extracellular regulated kinase 5 mediates osteoporosis through modulating viability and apoptosis of osteoblasts in ovariectomized rats. *Biosci Rep*. 2019;39(9). doi:10.1042/BSR20190432